Biofunctional hybrid materials: bimolecular organosilane monolayers on FeCr alloys

Leena Vuori[1], Jenni Leppiniemi[2,3], Markku Hannula[1], Kimmo Lahtonen[1], Mika Hirsimäki[1], Ergo Nõmmiste[4], Leila Costelle[1], Vesa P. Hytönen[2,3,5] and Mika Valden[*,1]

[1] Surface Science Laboratory, Optoelectronics Research Centre, Tampere University of Technology, PO Box 692, FI-33101 Tampere, Finland

[2] Institute of Biomedical Technology, Biokatu 6, FI-33104 University of Tampere and Tampere University Hospital, Tampere, Finland.

[3] BioMediTech, Biokatu 10, FI-33520 Tampere, Finland.

[4] Institute of Physics, University of Tartu, Riia 142, EE-51014 Tartu, Estonia.

[5] Fimlab Laboratories Ltd., PO Box 66, FI-33520 Tampere, Finland.

Hybrid organic-inorganic interfaces are the key to functionalization of stainless steel (SS). We present a solution-based deposition method for fabricating uniform bimolecular organosilane monolayers on SS and show that their properties and functionalities can be further developed through site-specific biotinylation. We correlate molecular properties of the interface with its reactivity via surface sensitive synchrotron radiation mediated high-resolution photoelectron spectroscopy (HR-PES) and chemical derivatization (CD), and demonstrate specific bonding of streptavidin proteins to the hybrid interface. The method facilitates efficient growth of uniform bimolecular organosilane monolayers on SS under ambient conditions without the need to prime the SS surface with vacuum-deposited inorganic buffer layers. The obtained insights into molecular bonding, orientation and behaviour of surface-confined organofunctional silanes on SS enable a new generic approach to functionalization of SS surfaces with versatile nanomolecular organosilane layers.

*To whom correspondence should be addressed. E-mail: mika.valden@tut.fi

1. INTRODUCTION

The potential benefits of nanotechnology are enormous. In addition to existing technologies that rely on nanoscale materials and phenomena, such as semiconductor devices and catalysts, nanomaterials hold a great promise for applications in many other technological fields [1]. Nanocoating technologies, or smart coatings, have been extensively researched to effect breakthroughs in wearable electronics, superomniphobic surfaces, biosensing and, for instance, self-healing nanocomposites for building structures [2-5]. Similarly, pressing environmental concerns have stimulated increasing interest in utilizing carbon nanotubes as a functional material in clean water technology [6]. The common trait in such applications is that their novel functionalities depend on nanoengineered surfaces and interfaces.

Here, we report on a nanomolecular approach (Figure 1) to fabricating an affordable, uniform and highly versatile hybrid interface consisting of a *bimolecular organosilane monolayer* on stainless steel (SS) surface. The present study is the first investigation to date to report on a realization of biofunctionality on SS achieved solely by utilizing electrochemistry and solution-based deposition techniques. Furthermore, in contrast to most previous efforts, we attain deep quantitative insights into the chemical bonding, molecular orientation and morphology in the silane layer at every stage of its fabrication. The quantitative spectroscopic information obtained with surface sensitive analytical techniques is utilized in the optimization of the hybrid interface composition to facilitate further surface functionalization via site-specific bonding of biotinylated poly-ethylene glycol (PEG) chains and streptavidin (SA) proteins.

SS is a ubiquitous, affordable and durable material with excellent thermal and mechanical properties. It is corrosion resistant due to its native and self-healing 5–10 nm thick passive oxide film that also makes a number of SS grades *in vivo* biocompatible [7-8]. Consequently, SS has already been utilized in applications like orthopaedic implantology, cardiovascular stents and biofilm resistant surfaces that require bio*compatibility* [9-10]. Bio*functionality on* SS is, however, still relatively unexplored, even though in harsh environments (*e.g.* food processing industries or biorefining processes), the inherent mechanical strength and corrosion resistance of an SS substrate would be an obvious advantage. The near total lack of rigorous studies on biofunctionalization of SS (Ref. 11 being a rare exception) is an indicative of how the progress in the field is constrained by the lack of detailed knowledge on the dynamic physicochemical interactions between inorganic surfaces and complex, biologically relevant molecules such as proteins or DNA [12].

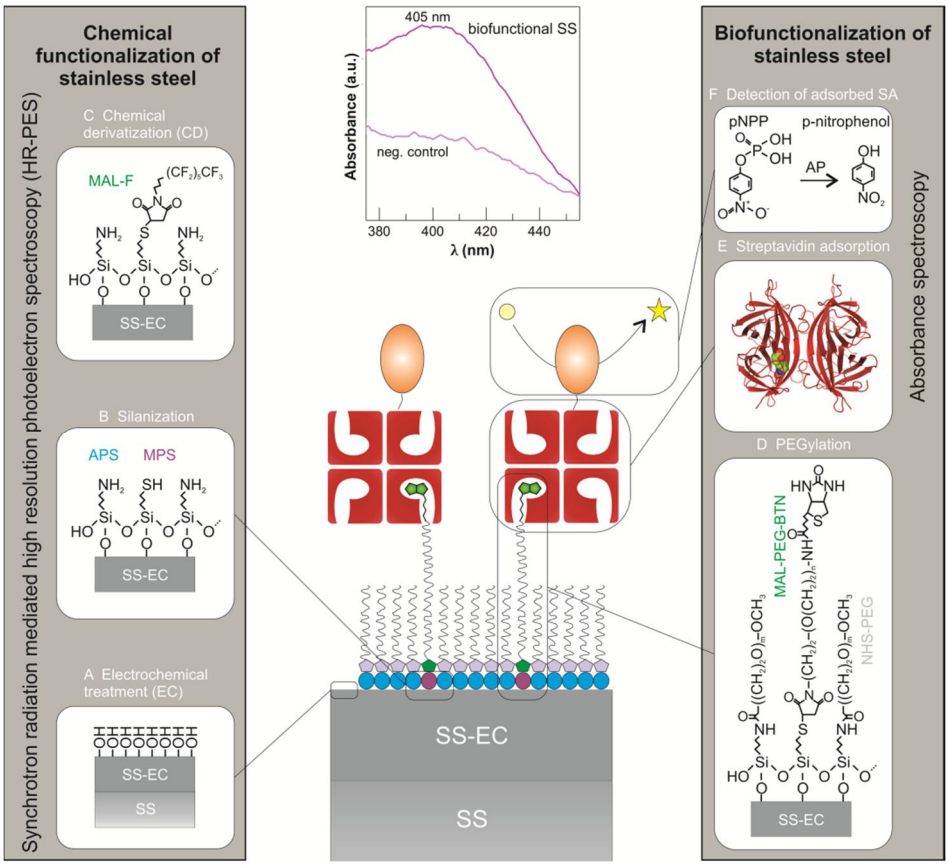

Figure 1. The approach to biofunctionalization of stainless steel. The column on the left illustrates the steps taken in the preparation of a stainless steel (SS) surface that is receptive for biofunctionalization: (A) The SS surface is electrochemically treated in order to remove impurities and increase the surface hydroxyl concentration (SS–EC). (B) SS–EC surface is silanized with a mixture of (3-aminopropyl)trimethoxysilane (APS) and (3-mercaptopropyl)trimethoxysilane (MPS). (C) The orientation of MPS thiol termini is determined via chemical derivatization (CD) with N-(4,4,5,5,6,6,7,7,8,8,9,9,9-tridecafluorononyl)maleimide (MAL–F). The surface properties are investigated by utilizing synchrotron radiation mediated high resolution photoelectron spectroscopy (HR-PES). The column on the right illustrates the steps required to demonstrate how the silanized SS can be further *bio*functionalized: (D) the silanized surface is PEGylated with polyethylene glycol succinimidyl ester (NHS–PEG) and maleimide-PEG-biotin (MAL–PEG–BTN). (E) The surface is exposed to streptavidin-alkaline phosphatase conjugates (SA–AP) that exhibit strong affinity to the biotin terminus in MAL–PEG–BTN. (F) Biotin-bound SA-AP conjugates are detected with p-nitrophenylphosphate (pNPP). In the presence of AP, pNPP is catalysed into p-nitrophenol, which absorbs light at 405 nm. The absorbance spectra of biofunctionalized SS and a negative control sample are shown in the top-middle inset.

Silanes, in turn, are excellent compounds for creating organic–inorganic interfaces. They are economic and environmentally benign. Furthermore, they exhibit strong covalent bonding with surface hydroxyls and there is an enormous variety of functionalized silanes available for tailoring surface properties of materials. However, unlike on materials such as silicon [13-14], silica [15-16] and glass [17], fabricating a uniform nanoscale silane layer on SS is challenging due to the absence of naturally occurring surface hydroxyls that facilitate efficient silane adsorption [18]. Furthermore, competition between Si–O–M (M = surface metal atom) and Si–O–Si bond formation on SS tends to lead to detrimental clustering and growth of a thick and non-uniform silane layer. Clustering and non-uniformity in a silane layer can, however, be alleviated by modifying the SS surface prior to silanization. For instance, in the report by Slaney *et al.*, SS surfaces were first primed with a nanolayer of silica via atomic layer deposition (ALD), and bimolecular silane layers were subsequently deposited on silica covered SS to create a surface that has potential for biomedical applications [11].

We, however, have shown that a receptive SS surface for a thin, uniform and strongly bound *monomolecular* silane layer can be created simply via electrochemical (EC) treatment of SS in weak sulphuric acid [19]. Here, we utilize the same approach to create, under ambient conditions, robust and uniform nanomolecular monolayers of *bimolecular* silane featuring a tuneable mixture of reactive amino- and thiol-groups. While bimolecular silane layers offer more versatility, their behaviour and properties are less well known in comparison to monomolecular silane layers [20-24]. In this paper, we gain insights into the growth and behaviour of the layer and show how it can be further utilized to effect biofunctional properties on stainless steel.

2. METHODS

Materials. Electrochemically polished EN 1.4372 (ASTM/AISI 201, Fe-18Cr-6Mn-4Ni) stainless steel (SS) was manufactured by Outokumpu Stainless Oy (Finland) and laser cut into samples with diameter of 9 mm and thickness of 1 mm by Jaloterässtudio, Finland. Sulphuric acid (A.C.S. reagent 95-98% H_2SO_4), N-(4,4,5,5,6,6,7,7,8,8,9,9,9-tridecafluorononyl)maleimide (MAL-F), dimethyl sulfoxide (DMSO) and tris(2-carboxyethyl)phosphine hydrochloride (TCEP) used prior to chemical derivatization were purchased from Sigma–Aldrich (St. Louis, MO, USA) and 3-aminopropyl trimethoxysilane (APS, $NH_2(CH_2)_3Si(OCH_3)_3$) and 3-mercaptopropyl trimethoxysilane (MPS, $SH(CH_2)_3Si(OCH_3)_3$) from Alpha Aesar, Germany. Maleimide-PEG-Biotin (MAL–PEG–BTN, MW 2000 Da) and PEG succinimidyl ester (NHS–PEG, MW 1000 Da) were ordered from Nanocs Inc. (New York, NY, USA). TCEP in biorecognition assay and phosphatase substrates (pNPP) were purchased from Sigma–Aldrich. Streptavidin- Alkaline Phosphatase (SA-AP) was from Roche Diagnostics GmbH (Mannheim, Germany) and D-biotin was from Fluka Chemie GmbH (Buchs, Switzerland).

Overview of the synthesis technique. As shown earlier in Figure 1, our approach to creating new functionalities on SS surface relies on understanding and controlling the properties of a bifunctional organosilane monolayer on SS and step-by-step deposition of further molecules with specific functional groups. In the first two steps, surface hydroxylation (A) and silanization (B), we create a uniform bimolecular organosilane monolayer that provides specific functional groups for further functionalization. An electrochemically polished stainless steel substrate is first hydroxylated by electrochemical treatment in weak sulphuric acid followed by deposition of a mixed silane layer on SS from a hydrolysis solution consisting of 3-aminopropyl trimethoxysilane (APS) and 3-mercaptopropyl trimethoxysilane (MPS) using different solution concentrations. Surface-confined MPS acts as a reactive component inside an APS matrix which, in turn, passivates the remaining surface area towards non-specific adsorption. The chemical derivatization (CD) experiment (step C) is conducted to assess the reactivity of the silane layer towards maleimide. In the fourth step (D), hetero-bifunctional maleimide-PEG-biotin (MAL-PEG-BTN) and NHS-PEG chains are co-adsorbed at the APS/MPS – SS interface. The maleimide termini in MAL-PEG-BTN couple exclusively with MPS and the tuneable concentration and dispersion of MPS is used to optimize the steric clearance between MAL-PEG-BTN chains and, consequently, large (~5 nm) SA proteins to be deposited later. NHS–PEGs bond preferentially with APS, thereby further passivating the remaining surface area. In the two final steps, we couple SA with the surface-confined biotinylated PEG compounds (step E) and demonstrate site-specific adsorption of SA proteins on the surface (step F). SA protein, a bacterial analogue of chicken avidin protein, was chosen for the demonstration, because it offers a robust and versatile molecule for easy and predictable functionalization without the need for specialized equipment [26-27].

Hydroxylation. The SS samples were sonicated for 10 minutes both in ethanol and deionized (DI) water in room temperature (RT, 22±1 °C). The electrochemical (EC) treatment was performed with Autolab PGSTAT12 potentiostat/galvanostat (Eco Chemie B.V., The Netherlands). In the EC treatment, the sample was placed in three-electrode electrochemical cell using an Ag/AgCl electrode and a Pt rod as a reference and a counter electrode, respectively. The SS surface was then reduced in order to remove surface impurities and the native oxide film in deaerated aqueous solution of 0.1 M sulphuric acid by applying a cathodic current of 5 mA/cm^2 for 5 min. The treatment was continued with passivation in the same solution at a constant potential of Ep = -0.197 V against the Ag/AgCl electrode for 10 min. The passivated sample was rinsed with DI water and blown dry with N_2.

Silanization. The silanization procedure was slightly modified from earlier investigations [19,28]. APS and MPS were hydrolysed in a same hydrolysis solution of 3:1 DI H_2O:EtOH solution for 60 s. The freshly prepared SS–EC surface was exposed to APS/MPS mixture in hydrolysis solution for 60 s followed by removal of excess solution with dry nitrogen flow. The samples were annealed for 10 min at 373 K in atmospheric conditions prior to transfer to UHV for HR-PES experiments. The silanization reaction

pathways are reported in detail in Ref. 28. Briefly, hydrolysis leads to formation of silanols ($R(CH_2)_3Si(OH)_3$). Under optimal conditions, a single silanol molecule adsorbs on the substrate with R group oriented outwards as hydrogen bonds between surface and silanol OH groups are created. The silanols may also oligomerize in the hydrolysis solution due to the formation of Si–O–Si-bonds in solution [28]. The adsorption behaviour also depends on the silane, temperature, pH, and the amount of water in the hydrolysis solution [28,29]. According to Chovelon *et al.* annealing a silanized sample in ambient conditions at ca. 373 K leads to covalent bond formation between silane molecules and SS surface (Si–O–M). The thiol (SH) groups in MPS may also form disulphide (S-S) bonds with each other at 373 K, but these detrimental bonds were broken by incubating the samples in tris(2-carboxyethyl)phosphine (TCEP) [17].

Chemical derivatization (CD). Prior to CD experiments the silanized sample was exposed to 0.05 M TCEP solution for 15 min in order to reduce any potential S-S bonds between surface-confined silane thiol-groups. The surface was then rinsed with water and dried with N_2. For CD experiments, samples were then exposed to a 0.5 M MAL–F solution in DMSO for 60 min, followed by rinsing with DMSO and drying with N_2. MAL-F bonds preferentially with thiol-groups. Therefore, measuring the residual F on the surface after MAL-F exposure gives an indication of the number of available MPS sites and their reactivity towards MAL-PEG-BTN (to be used later in biofunctionalization experiments).

High resolution photoelectron spectroscopy (HR-PES). In the investigation of bimolecular silane monolayers it is essential to employ surface sensitive photoelectron spectroscopy [25], since scanning probe techniques are not readily applicable to the investigation of chemical bonding and most optical and electron microscopy techniques are not sufficiently surface sensitive to allow straightforward analysis of nanomolecular monolayers. The samples were investigated before and after CD with HR-PES at MAX IV Laboratory (Lund University, Sweden) at beamline D1011 [30]. In short, D1011 is a bending magnet beamline equipped with a modified SX-700 plane grating monochromator. The HR-PES spectra were measured by an electron energy analyser SCIENTA SES-200 in a fixed analyser transmission (FAT) mode with 200 eV pass energy and normal emission. The photon flux on the sample was ~10^{11} photons/s, the total energy resolution was ~200 meV and the sampled surface area was approximately 0.20 mm^2. The synchrotron radiation was linearly polarized in all experiments which were conducted with three primary photon energies: $h\nu_1$=1486.6 eV, $h\nu_2$=720 eV and $h\nu_3$=300 eV. Complementary experiments were also conducted with photon energies of 550 eV and 900 eV. The surface morphology of silanized SS surfaces before and after CD was determined by inelastic electron energy-loss background (IEEB) analysis [31,32] using the implementation in QUASES-Tougaard software package [33]. The method relies on accurate description of photoelectron energy-loss background due to inelastic scattering of the photoemitted electrons. A more detailed description of the initial silane deposition, PES experiments (e.g. calibration,

background subtraction and radiation induced damage) and IEEB analysis can be found in Supplementary Data.

Biofunctionalization. First, TCEP was diluted in water and 80 µL of 50 mM TCEP solution was incubated on the surface for 20 min at RT. Then, TCEP solution was removed and 40 µL of 10 mM MAL–PEG–BTN in PBS buffer (pH 7.4) was added and incubated for 10 min. This was followed by the addition of 40 µL of NHS–PEG in PBS and incubation was continued for one hour. After PEGylation, the surface was rinsed three times with 300 µL of PBS-Tween 0.05%. The unoccupied sites at the surface were blocked by incubating in 300 µL of 5% milk-PBS-Tween 0.05% for one hour at RT to reduce the amount of non-specific bonding of SA-AP. Then the surface was once again rinsed three times with 300 µL PBS-Tween.

Detection of biotin. 80 µL of Streptavidin alkaline phosphatase (SA–AP) conjugate was pipetted onto the surface and incubated for one hour at RT. To remove any non-reacted SA–AP, the surfaces were rinsed six times with 300 µL PBS-Tween. Samples were protected from light and 30 µL of phosphatase substrate (pNPP 1 mg/mL in 1 M diethanolamine (DEA) buffer, pH 9.8, containing 0.5 mM $MgCl_2$) was applied onto the centre of the surface. 2 µL samples were obtained for the determination of UV/Vis-spectrum (NanoDrop 1000 Spectrophotometer, Thermo Scientific, Wilmington, DE, USA) 10, 20, 30, 40, 60 and 120 minutes after addition of pNPP.

Control experiment. SA-AP was incubated with free biotin prior addition to the surface in order to inhibit its affinity towards surface-confined biotin. The substrate pNPP was also reacted with metal surface that was rinsed only with PBS-Tween prior addition of pNPP, to analyse whether metal itself can catalyse the reaction of pNPP to para-nitrophenol.

3. RESULTS AND DISCUSSION

Our initial finding after hydroxylation and silanization (Figures 1A and 1B) was that while the surface silanization with APS and MPS was efficient (Supplementary Data, Figure S2) and reproducible, the surface chemistry was more complicated in comparison to a monofunctional APS layer [19]. In particular, we observed that although the relative surface concentration of deposited APS and MPS did correlate with the relative concentration of APS and MPS in the hydrolysis solution, the correlation was not linear (Supplementary Data, Table S1). Similar behaviour was observed earlier by Jones *et al.*[25] In order to be able to predict the APS/MPS surface concentration ratio in the silane film from the composition of the hydrolysis solution, an investigation of layer composition and morphology was conducted as a function of MPS concentration in the solution. MPS concentration in hydrolysis solution was varied between 0.01 and 1.00 v-% while the APS concentration was maintained constant at 0.10 v-%. The two most interesting layers were selected for further study.

Figure 2A presents O 1s photoelectron spectra for SS-EC silanized with 0.10 v-% APS / 0.01 v-% MPS solution ratio (SIL1) and 0.10 v-% APS / 1.00 v-% MPS solution ratio (SIL2). The experiments were conducted after steps in Figures 1A and 1B by employing photon energy of 720 eV and the corresponding information depth is shown schematically in the top-right corner. At this photon energy the majority of PES signal originates from the silane layer, but there is also a contribution from the underlying SS-EC substrate. As expected, both spectra exhibit features that indicate the presence of Si–O–Si and Si–O–M bonds, and SO_4 (residue from EC treatment) at 532.4 eV and free surface OH (531.4 eV) and metal oxides (530.0 eV) [19,34]. There are also minor signals from impurities originating from sample preparation in ambient conditions, such as C=O and C–O and silicon oxides from the underlying SS-EC. The prominent Si–O signal indicates the formation of a surface confined silane overlayer.

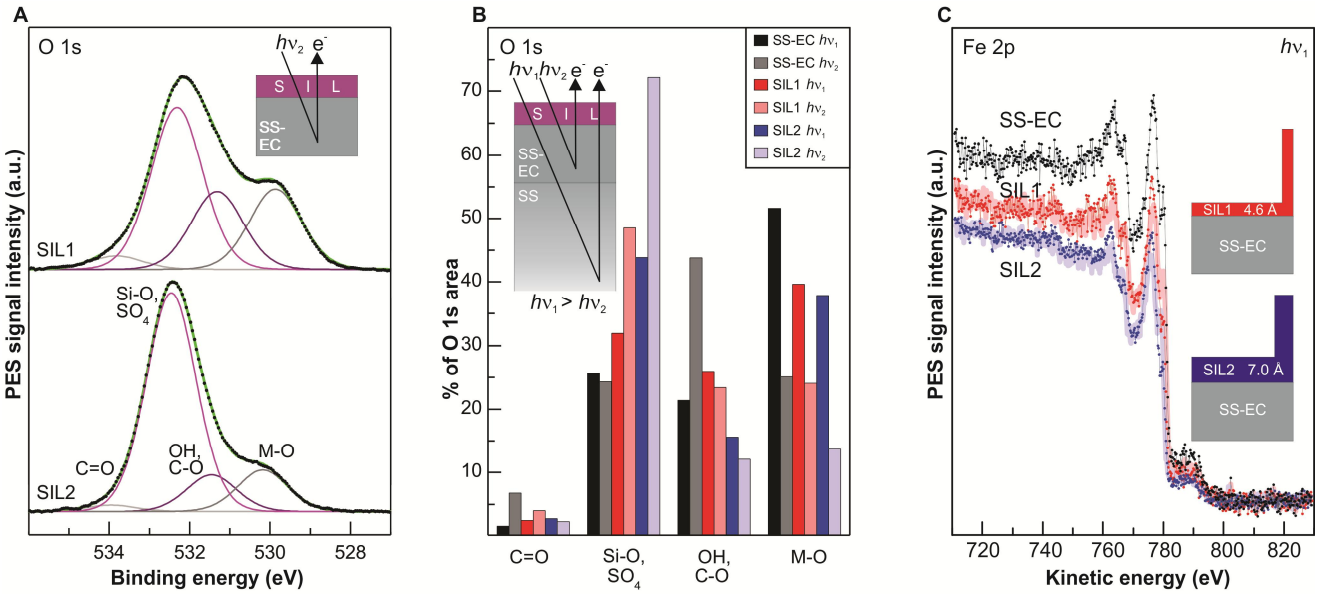

Figure 2. HR-PES results of O 1s spectra and IEEB analysis. (A) The HR-PES O 1s spectra of samples SIL1 (0.10 v-% APS / 0.01 v-% MPS, top) and SIL2 (0.10 v-% APS / 1.00 v-% MPS, bottom). The schematic illustration demonstrates the information depth of emitted electrons in HR-PES experiments with photon energy $h\nu_2$ of 720 eV. The experimental spectra are shown as dotted lines. The fits indicate the presence of surface-bound OH, SS metal oxides, SO_4 and Si-O-(Metal) bonds as well as states related to residual atmospheric impurities such as C=O and C-O. The envelope of fitted components is shown in solid green. (B) The different components in O 1s spectra for SS-EC, SIL1 and SIL2 are shown in percentages of total O 1s signal. The inset demonstrates the difference between information depths for the two photon energies ($h\nu_1$ = 1486.6 eV and $h\nu_2$ = 720 eV). (C) The inelastic electron energy-loss background (IEEB, see Supplementary Data for details) analysis of Fe 2p region of the reference sample SS-EC (black), SIL1 (red) and SIL2 (blue). Spectra were obtained with photon energy of 1486.6 eV. A good fit between experimental (solid lines) and modeled (dotted line) data is achieved with the surface morphologies shown by the schematic illustrations.

Moreover, the analysis of spectral features in O 1s signal allows quantification of different oxygen bonds present on the surface. Figure 2B illustrates the observed bonds and their quantities on SIL1, SIL2 and SS-EC as measured by employing two photon energies ($h\nu_1$ = 1486.6 eV and $h\nu_2$ = 720 eV). Data from SS-EC shows surface composition prior to silanization. The inset graph demonstrates the respective surface sensitivities

for $h\nu_1$ and $h\nu_2$. The relative OH concentration on SS-EC indicates that the surface has been successfully hydroxylated. Furthermore, the OH groups are clearly confined only to the topmost surface region, since the OH signal is enhanced at the lower, more surface sensitive, photon energy $h\nu_2$. In contrast, SO_4 residue from the EC treatment is evenly distributed in the subsurface region as shown by the relatively constant SO_4 concentration.

On the two silanized surfaces, SIL1 and SIL2, the most obvious result is the enhanced concentration of silane related Si–O bonds. By comparing the quantity of Si–O bonds on the two surfaces, it is evident that SIL2 has a higher concentration of silane species. Although Si–O signal overlaps with the minor SO_4 feature from the substrate, the concomitant decrease in OH and M-O concentrations and the increase in Si–O concentration (along with an increase in the Si 2p peak intensity as shown in Supplementary Data Figure S3A) on SIL2 all indicate that the total silane concentration was higher on SIL2 than on SIL1. The increase in the quantity of Si–O bonds observed at lower photon energy confirms that silane layers are confined to the surface on both SIL1 and SIL2.

The morphology of an ideal silane layer for PEGylation would feature a uniform and well-ordered bimolecular monolayer with amino- and thiol-groups pointing out of the surface plane. To determine the overall morphology of our silane layer, we employed inelastic electron energy-loss background (IEEB) analysis developed by Tougaard [31,32]. Briefly, it facilitates the determination of surface morphology and composition through comparison of experimental IEEB data and computational IEEB predictions obtained from surface morphology models and experimental parameters. Since all the analysed spectra are acquired from an area of approximately 0.20 mm^2, the results are statistically averaged and represent a significant sample area for practical applications. We have employed IEEB analysis previously in the quantitative investigations of Fe–Cr alloy surfaces and silane layers [19,35-37]. The data measured from the SS-EC surface was employed as a reference and the APS/MPS layer morphology was determined from the IEEB of Fe 2p signal [25].

Figure 2C shows the best IEEB fits to experimental data and, as indicated in the schematic models on the right, the majority of the surface area is covered by 4.6 Å (SIL1) and 7.0 Å (SIL2) thick silane layers. Both results are in the same range as the values published earlier for APS on SS and silica [19,29,38]. The remaining surface area on SIL1 and SIL2, presented as taller blocks in the models, corresponds to regions of siloxane clustering. It can be readily seen that SIL2 features a thicker silane layer and exhibits more clustering. This is a natural consequence of the higher silane concentration in the hydrolysis solution: higher concentration increases the probability of oligomer formation and the adsorption of incompletely hydrolysed MPS, which leads to the observed increase in detrimental clustering and enhanced formation of non-specific siloxane bonds.

Since MPS surface compounds are intended to act as coupling agents for MAL–PEG–BTN (Figure 1D), and eventually SA protein, an important criterion for a functional silane layer is the presence of sterically and chemically available surface-bound thiol groups. Too densely packed MPS sites would result in a dense MAL–PEG–BTN arrangement which, in turn, would sterically hinder the efficient bonding of large biotin–SA complexes. In addition to surface density of MPS, it is of an utmost importance to ascertain whether the thiol groups in MPS are chemically receptive towards MAL–PEG–BTN.

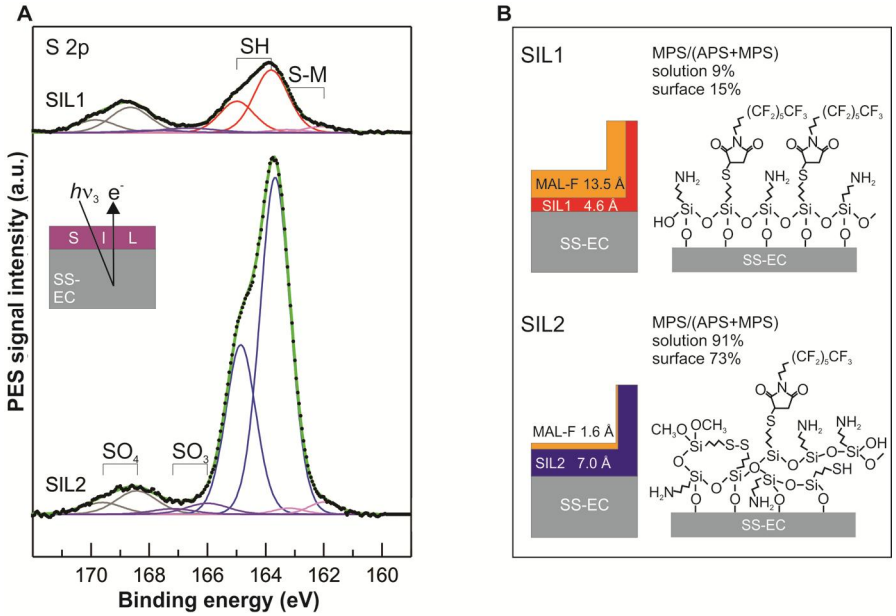

Figure 3. HR-PES results showing S 2p spectra and IEEB analysis after chemical derivatization (CD). (A) S 2p spectra from samples SIL1 (top) and SIL2 (bottom) with fits indicating the presence of SH, S-Metal (S-M) and S–S bonds as well as SO_3 and SO_4. The schematic inset demonstrates the information depth in HR-PES experiments with photon energy $h\nu_3$ of 300 eV. (B) Results from IEEB analysis shown as schematic drawings for SIL1 and SIL2 before (red and blue, corresponding to spectra in Figure 3A) and after (orange) CD. The MPS/APS ratios on the surface are determined from the HR-PES spectra measured with photon energy of 550 eV. The schematic illustrations on the right show the proposed monolayer configuration of SIL1 (top) and clustered thicker overlayer of SIL2 (bottom). For clarity, some Si-O-bonds are omitted from the figure.

Figure 3A shows HR-PES S 2p signal from SIL1 and SIL2 as measured by utilizing photon energy (300 eV) that was optimized for S detection with high surface sensitivity. S 2p peaks comprise of S $2p_{3/2}$ and S $2p_{1/2}$ transitions with a binding energy difference of 1.18 eV and area ratio of 2:1. The S $2p_{3/2}$ peak at 163.7 eV originates from thiol (SH) and S–S bonds of MPS. The peak at 168.5 eV indicates SO_4 residue in the underlying SS-EC. Minor components are observed at 166.3 eV (SO_3, from reduced sulphates) and at 162.0 eV (most likely S-Metal bonds). Thiol groups are clearly present on both surfaces, but the most striking observation is that the concentration of thiol groups on SIL2 (blue curves) is 4.7 times higher than on SIL1 (red curves).

The chemical availability of the surface-confined thiol groups was assessed in chemical derivatization (CD) experiments (Figure 1C). In CD, the surface is treated with label molecules that readily react with a targeted functional group on the surface (in this case, thiols) and can thereby be easily detected [39]. In our CD experiments, we employed fluorocarbon labelled maleimide (MAL–F). The samples were incubated in tris(2-carboxyethyl)phosphine hydrochloride (TCEP) solution prior to CD experiments in order to break the any S-S bonds on the surface prior to the adsorption of MAL-F. Maleimide exhibits strong affinity towards thiol groups in MPS, but is, under the present experimental conditions, inert towards the amino groups of APS. Since fluorine is not present either in SS or in silanes, the concentration of covalently bound MAL–F, and thus the chemical availability of thiols groups, can be estimated from the F 1s signal and increase in the maleimide overlayer thickness. Figure 3B shows that after MAL–F treatment the observed increase in the maleimide layer thickness on SIL2 was 1.5 Å whereas on SIL1 it was 13.5 Å. A corresponding trend could also be seen in the F 1s signal (see Supplementary Data, Figure S3B).

The results in Figures 2 and 3 indicate that SIL1 is, indeed, a uniform, bimolecular silane monolayer with the majority of the SH termini in a correct upright configuration and, thus, sterically and chemically available for MAL-PEG-BTN bonding. In contrast, on SIL2 we observe a thicker silane layer but, somewhat surprisingly, greatly reduced uptake of MAL-F in comparison to SIL1. We attribute the enhanced uptake of MAL-F on SIL1 to the ability of surface-bound OH groups to orient the first layer of silane molecules so that the functional groups point out of the surface plane. However, if – as on SIL2 – the silane thickness exceeds one monolayer the silane–silane interaction starts to dominate and, as a consequence, multilayers grow in a less orderly fashion. Hence, even though there are considerably more thiol groups on SIL2 (Figure 3A), the weaker orientation of functional groups offers fewer available bonding sites for maleimide. This is illustrated in Figure 3B by schematic diagrams of our proposed molecular structures for SIL1 and SIL2. The qualitative diagrams are based on recent results [29,38-40] and the analysis of chemical bonds we have observed with HR-PES. Our PES experiments indicate successful coupling of the bi-molecular silane film to the surface. Further insights into the adsorption geometry and bonding on the surface will be obtained by atomic force microscopy (AFM) and Fourier transform infrared spectroscopy (FTIR) in the forthcoming more detailed studies of the biofunctional properties. The identified correlation between the molecular structure of silane layer and its reactivity towards maleimide is a finding that underscores the importance of understanding and controlling the molecular adsorption geometry of interface structures in nanoscale functional films.

To demonstrate the functional properties of our layer, we fabricated a set of silanized surfaces with SIL1 silanization parameters and PEGylated (Figure 1D) them with hetero-bifunctional MAL–PEG–BTN (molecular weight MW = 2000 Da) and NHS–PEG (MW = 1000 Da) molecules. In comparison to other reactive groups used for bioconjugation (*e.g.* NHS), maleimide groups exhibit particularly good stability for

thiol coupling [41]. Hence, MAL–PEG–BTN will bond preferentially, *via* its maleimide group, to the thiol groups on the surface. At its other end, MAL–PEG–BTN terminates in a biotin group to which SA is known to link through strong hydrogen bonding (Figure 1E) [27]. NHS–PEG, in turn, carries an amino-reactive (NHS) group that bonds covalently with the amino terminus in surface-bound APS. Therefore, NHS–PEGs cover the remaining surface area and function as inert spacer molecules between MAL–PEG–BTN sites, thus preventing non-specific protein adsorption between the biotinylated sites [42-44]. MAL–PEG–BTN features a linear PEG chain that is almost twice the length of NHS–PEG. Since PEGs can be synthesized with a relatively low polydispersity, we expect the biotin group in MAL–PEG–BTN to protrude clearly above NHS–PEGs and, thus, be readily available for bonding with SA.

The overall performance of the biotinylated nanomolecular interface was confirmed by exploiting strong and specific SA-biotin interaction [27]. Streptavidin conjugated alkaline phosphatase (SA-AP) was deposited on the surface using P-nitrophenylphosphate as a substrate for AP. The yellow product (p-nitrophenol) of the reaction catalysed by AP was measured by absorbance at 405 nm (Figure 1F and top middle inset) [25].

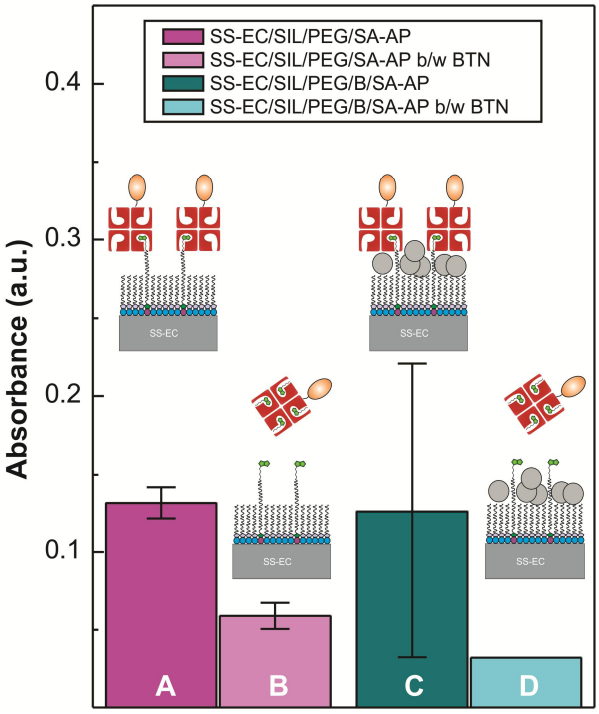

Figure 4. SA-AP uptake as determined from biorecognition assay experiments on silanized and PEGylated SS-EC/SIL1 surfaces (SS-EC/SIL1/PEG). (A) Uptake of SA-AP on SS-EC/SIL1/PEG surface. (B) Uptake of biotin (BTN) saturated SA-AP on SS-EC/SIL1/PEG. Absorbance spectra from experiments A and B are shown in Figure 1 (top middle inset). Two additional negative control samples were prepared in order to investigate non-specific adsorption of SA-AP. (C) SA-AP uptake on SS-EC/SIL1/PEG surface that was blocked with milk proteins. (D) Uptake of biotin-saturated SA-AP on SS-EC/SIL1/PEG surface that was blocked with milk proteins. The error bars indicate measured standard deviation.

As indicated by the biorecognition assay results in Figure 4, PEGylated surface does, indeed, exhibit specific reactivity towards SA. A freshly PEGylated surface was first exposed to unsaturated (A) and biotin-saturated SA-AP (B). Saturating SA-AP with biotin prior to deposition clearly reduced its uptake in comparison to unsaturated SA-AP. The same two experiments were also conducted on surfaces pre-covered with milk protein (C and D) in order to probe non-specific protein adsorption behaviour. When the surface was blocked with milk proteins, we observed more variation in the quantity of surface-bound SA–AP. We postulate that the milk proteins form a loosely bound and weakly ordered layer that sterically blocks SA–AP bonding to biotin termini. By comparing results from experiments B and D, we conclude that the saturation of SA-AP with biotin prior to its deposition clearly inhibits its bonding both in the absence and presence of milk proteins, thus providing more evidence for the specificity of the reaction with MAL–PEG–BTN.

4. CONCLUSIONS

We have demonstrated a solution-based technique for economic and effective fabrication of bi-functional organosilane monolayers for functionalization of stainless steels. Furthermore, we have elucidated the nanoscale structure and composition of the organosilane layer by applying quantitative surface sensitive analytical techniques. This has allowed us to correlate the properties of the silane solution with the structure and composition of a surface-confined organosilane layer (e.g. the relative concentration of active MPS sites). The bifunctional layer, in turn, has been shown to provide a versatile avenue for enabling wide range of biotin-avidin based biochemistry on SS surfaces via tuning of the molecular structure and composition of the bimolecular silane overlayer and functionalized PEGs. As we have shown here, SA proteins (or its variants [45,46]) could be bound to the biotinylated organosilane layer, thereby facilitating further surface functionalization by thousands of commercially available biotinylated molecules with affinity towards SA. Moreover, although not demonstrated here, the covalent bonding of silanes and PEGs to the surface also makes it possible to chemically erase the SA layer without destroying the silane–PEG layer thereby regenerating the surface. The system studied in this paper can be tailored, for example, to fabricate a wide variety of biosensors by using specific avidin-conjugated molecules. This type of sensors could be used e.g. in food and medical industry to recognize unwanted bacteria in the process system via selection of functional groups sensitive to e-coli bacteria, for instance. The bifunctional APS/MPS stainless steel can also be functionalized with any maleimide or n-succinimidyl ester terminated molecules. This enables for example specific binding of MAL-terminated RGD-peptides for enhanced cell binding. This type of approach could be exploited in pro-healing stents. Pro-healing stents enhance the attachment of right types of cells and tissue to the stent surface which would reduce the risk of encapsulation of the stent.

Finally, potential applications are not limited to avidin-biotin technology and biosciences only. Now that the bonding to and ordering in the nanomolecular monolayer has been elucidated, covalently-bound

bimolecular organosilane layers can be tailored to induce a variety of functionalities (*e.g.* superomniphobicity or anti-bacterial properties) by grafting them with suitable PEGs and functional groups. For instance, by functionalizing the silane layer with fluorocarbon groups, nanoscale anti-fouling coatings can be created. Our technique to fabricating well-ordered and –characterized silane layers also facilitates incorporation of robust and well-ordered nanoscale silane films on any hydroxyl-rich surfaces including light-emitting semiconductor materials or ceramic/glass surfaces to attain protective layers that are transparent to light. Hence, our approach - based on solution-based deposition techniques and profound understanding of molecular bonding mechanisms - offers a sophisticated, yet relatively efficient way of fabricating functional SS surfaces for a plethora of applications.

ACKNOWLEDGMENT

We acknowledge financial support by Academy of Finland (decision number 250324), the Finnish Funding Agency for Innovation (FIMECC Oy, HYBRIDS-programme, decision number 1236/13, 2105/31/2013), Estonian Ministry of Education and Research (target-financed theme IUT2-25) and Estonian Centre of Excellence: Materials for Sustainable Development and Estonian Science Foundation (grant 8737). The research leading to these results has also received funding from the European Community's Seventh Framework Programme (FP7/2007-2013) CALIPSO under grant agreement nº 312284. This work was partially supported by Finland Centennial Foundation Fund for the Association of Finnish Steel and Metal Products (L.V.), Finnish Academy of Science and Letters, Vilho, Yrjö and Kalle Väisälä Foundation (L.V.), Jenny and Antti Wihuri Foundation (L.V.) and Tampere Graduate Program for Biomedicine and Biotechnology (TGPBB) (J.L.). We are indebted to MAX IV Laboratory staff and, in particular, A. Preobrajenski for technical and scientific input. We also thank S. Kukkurainen for the SA image in Figure 1E, and U. Kiiskinen for excellent technical assistance.

REFERENCES

[1] Hsinchun C, Mihail C R, Xin L, Yiling, L 2008 Trends in Nanotechnology Patents *Nature Nanotech.* 3 123-125.

[2] Rogers J A, Someya T and Huang Y 2010 Materials and Mechanics for Stretchable Electronics *Science* 327 1603-1606.

[3] Pan S, Kota A K, Mabry J M and Tuteja A 2013 Superomniphobic Surfaces for Effective Chemical Shielding *J. Am. Chem. Soc.* 135 578-581.

[4] Martin C R and Siwy Z S 2007 Learning Nature's Way: Biosensing with Synthetic Nanopores *Science* 317 331-332.

[5] Fernández J E 2007 Materials for Aesthetic, Energy-Efficient, and Self-Diagnostic Buildings *Science* 315 1807-1810.

[6] Elimelech M and Phillip W A 2011 The Future of Seawater Desalination: Energy, Technology, and the Environment *Science* 333 712-717.

[7] Bordji K, Jouzeau J-Y, Mainard D, Payan E, Delagoutte J-P and Netter P. 1996 Evaluation of the effect of three surface treatments on the biocompatibility of 316L stainless steel using human differentiated cells *Biomaterials* 17, 491-500.

[8] Diaz M, Sevilla P, Galán A M, Engel E and Gil F G 2008 Evaluation of ion release, cytotoxicity, and platelet adhesion of electrochemical anodized 316 L stainless steel cardiovascular stents *J. Biomed. Mater. Res. Part B* 87B 555-561.

[9] Caro A, Humblot V, Méthivier C, Minier M, Barbes L, Li J, Salmain M and Pradier C-M 2010 Bioengineering of stainless steel surface by covalent immobilization of enzymes. Physical characterization and interfacial enzymatic activity *J. Colloid Interface Sci.* 349 13-18 (2010).

[10] Caro A, Humblot V, Méthivier C, Minier M, Salmain M and Pradier, C-M 2009 Grafting of lysozyme and/or poly(ethylene glycol) to prevent biofilm growth on stainless steel surfaces *J. Phys. Chem. B* 113 2101-2109.

[11] Slaney A M, Wright V A, Meloncelli P J, Harris K D, West L J, Lowary T L and Buriak, J M 2011 Biocompatible Carbohydrate-Functionalized Stainless Steel Surfaces: A New Method For Passivating Biomedical Implants *ACS Appl. Mater. Interfaces* 3 1601-1612.

[12] Koegler P, Clayton A, Thissen H, Santos G N C and Kingshott P 2012 The influence of nanostructured materials on biointerfacial interactions *Adv. Drug. Deliv. Rev.* 64 1820-1839.

[13] Wang M, Liechti K M, Wang Q and White J M 2005 Self-assembled silane monolayers: Fabrication with nanoscale uniformity *Langmuir* 21 1848-1857.

[14] Graf N, Yegen E, Gross T, Lippitz A, Weigel W, Krakert S, Terfort A and Unger W E S 2009 . XPS and NEXAFS studies of aliphatic and aromatic amine species on functionalized surfaces *Surf. Sci.* 603 2849-2860.

[15] Arroyo-Hernández M, Pérez-Rigueiro J and Martínez-Duart J M 2006 Formation of amine functionalized films by chemical vapour deposition *Mat. Sci. Eng. C* 26 938-941.

[16] Horr T J and Arora P S 1997 . Determination of the acid-base properties for 3-amino, 3-chloro and 3-mercaptopropyltrimethoxysilane coatings on silica surfaces by XPS *Coll. Surf. A: Physicochem. Eng. Asp.* 126 113-121.

[17] Pallavicini P, Dacarro G, Galli M and Patrini M 2009 Spectroscopic evaluation of surface functionalization efficiency in the preparation of mercaptopropyltrimethoxysilane self-assembled monolayers on glass *J. Colloid Interface Sci.* 332 432-438.

[18] Meth S and Sukenik C N 2003 Siloxane-anchored thin films on silicon dioxide-modified stainless steel *Thin Solid Films* 425, 49-58.

[19] Jussila P, Ali-Löytty H, Lahtonen K, Hirsimäki M and Valden M 2010 Effect of surface hydroxyl concentration on the bonding and morphology of aminopropylsilane thin films on austenitic stainless steel *Surf. Interface Anal.* 42 157-164.

[20] Moulton S, Liu X, Yue Z, Romeo T, Weber J, Scheuermann T and Wallace G 2013 Biofunctionalized anti-corrosive silane coatings for magnesium alloys *Acta Biomater.* 9 8671-8677.

[21] Kim H J, Kwon S-R and Kim K 2012 Electrochemically active cyclic disulfide-ended organic silane linkage for preparation of multi-biofunctional electrode surfaces *Electrochem. Comm.* 20 52-55.

[22] Park K and Jo S 2000 Surface modification using silanated poly(ethylene glycol)s *Biomaterials* 21 605-616.

[23] O'Brien P J, Shenogin S, Liu J, Chow P K, Laurencin D, Mutin P H, Yamaguchi M, Keblinski P and Ramanath G 2012 Bonding-induced thermal conductance enhancement at inorganic heterointerfaces using nanomolecular monolayers *Nature Mater.* 12, 118-122.

[24] Jones F R, Liu X M, Thomason J L, 2007 *The differential adsorption of silanes from solution onto model E-glass surfaces using high resolution XPS. In: Silanes and Other Coupling Agents* [Online]; VSP International Science Publishers, 29-37. http://strathprints.strath.ac.uk/6495/.

[25] Detailed descriptions of the methods are available on-line as Supplementary Data to this article.

[26] Wilchek M, Bayer E A, Livnah O 2006 Essentials of biorecognition: The (strept)avidin–biotin system as a model for protein–protein and protein–ligand interaction *Immunol. Lett.* 103 27-32.

[27] Laitinen O H, Nordlund H R, Hytönen V P and Kulomaa M S 2007 Brave new (strept)avidins in biotechnology *Trends Biotechnol.* 25 269-277.

[28] Chovelon J M, Aarch L E, Charbonnier M, Romand M 1995 Silanization of Stainless Steel Surfaces: Influence of Application Parameters *The Journal of Adhesion* 50 43-58.

[29] Krasnoslobodtsev A V and Smirnov S N 2002 Effect of water on silanization of silica by trimethoxysilanes *Langmuir* 18 3181-3184.

[30] Nyholm R, Svensson S, Nordgren J and Flodström A 1986 A soft X-ray monochromator for the MAX synchrotron radiation facility *Nucl. Instr. and Meth. A* 246 267-271.

[31] Tougaard S 2003 Quantification of Nanostructures by Electron Spectroscopy. In *Surface analysis by Auger and X-ray photoelectron spectroscopy*; Briggs, D.; Grant, J. T., Eds.; IM Publications and Surface Science Spectra, United Kingdom, 295-345.

[32] Tougaard S 2010 Energy loss in XPS: Fundamental processes and applications for quantification, non-destructive depth profiling and 3D imaging *J Electron Spectrosc. Relat. Phenom*. 178-179 128-153.

[33] Tougaard S 2003 QUASES: Software for Quantitative XPS/AES of Surface Nano-Structures by Analysis of the Peak Shape and Background – version 5.0; QUASES-Tougaard, Inc., Odense, Denmark. http://www.quases.com/.

[34] Bera S, Rangarajan S and Narasimhan S V 2000 Electrochemical passivation of iron alloys and the film characterisation by XPS *Corros. Sci.* 42 1709-1724.

[35] Ali-Löytty H, Jussila P and Valden M 2013 Optimization of the electrical properties of Ti–Nb stabilized ferritic stainless steel SOFC interconnect alloy upon high-temperature oxidation: The role of excess Nb on the interfacial oxidation at the oxide–metal interface *Int. J. Hydrogen Ener.* 38 1039-1051.

[36] Ali-Löytty H, Jussila P, Hirsimäki M and Valden M 2011 Influence of CrN surface compound on the initial stages of high temperature oxidation of ferritic stainless steel *Appl. Surf. Sci.* 257 7783-7791.

[37] Jussila P, Ali-Löytty H, Lahtonen K, Hirsimäki M and Valden M 2009 Inhibition of initial surface oxidation by strongly bound hydroxyl species and Cr segregation: H_2O and O_2 adsorption on Fe–17Cr *Surf. Sci.* 603 3005-3010.

[38] Chauhan A K, Aswal D K, Koiry S P, Gupta S K, Yakhmi J V, Sürgers C, Guerin D, Lenfant S and Vuillaume D 2008 Self-assembly of the 3-aminopropyltrimethoxysilane multilayers on Si and hysteretic current–voltage characteristics *Appl. Phys. A* 90 581-589.

[39] Graf N, Lippitz A, Gross T, Pippig F, Holländer A and Unger W E S 2010 Determination of accessible amino groups on surfaces by chemical derivatization with 3,5-bis(trifluoromethyl)phenyl isothiocyanate and XPS/NEXAFS analysis *Anal. Bioanal. Chem.* 396 725.

[40] van Ooij W J, Zhu D, Palanivel V, Lamar J A and Stacy M. 2006 Overview: The Potential of silanes for chromate replacement in metal finishing industries *Silicon Chem.* 3 11-30.

[41] Zimmermann J L, Nicolaus T, Neuert G and Blank, K. 2010 Thiol-based, site-specific and covalent immobilization of biomolecules for single-molecule experiments *Nature Protoc.* 5 975-985.

[42] Mrabet B, Mejbri A, Mahouche S, Gam-Derouich S, Turmine M, Mechouet M, Lang P, Bakala H, Ladjimi, M, Bakhrouf A, Tougaard S and Chehimi, M M 2011 Controlled adhesion of Salmonella Typhimurium to poly(oligoethylene glycol methacrylate) grafts *Surf. Interface Anal.* 43 1436-1443.

[43] Takao H. 2010 Biofunctionalization of titanium for dental implant *Jap. Dent. Sci. Rev.* 46 93-101.

[44] Alcantar N A, Aydil E S and Israelachvili J N 2000 Polyethylene glycol–coated biocompatible surfaces *J. Biomed. Mater. Res. B* 51 343-351.

[45] Määttä J A E, Eisenberg-Domovich Y, Nordlund H R, Hayouka R, Kulomaa M S, Livnah O and Hytönen V P 2011 Chimeric avidin shows stability against harsh chemical conditions – biochemical analysis and 3D structure *Biotechnol. Bioeng.* 108 481-490.

[46] Leppiniemi J, Määttä J A E, Hammaren H, Soikkeli M, Laitaoja M, Jänis J, Kulomaa M S and Hytönen V P 2011 Bifunctional Avidin with Covalently Modifiable Ligand Binding Site *PLoS ONE* 6 e16576.